Journal of Luminescence 155 (2014) 251–256

Contents lists available at ScienceDirect

Journal of Luminescence

journal homepage: www.elsevier.com/locate/jlumin

Interplay between chromium content and lattice disorder on persistent luminescence of $ZnGa_2O_4:Cr^{3+}$ for in vivo imaging

Suchinder K. Sharma [a], Aurelie Bessière [a], Neelima Basavaraju [b], Kaustubh R. Priolkar [b], Laurent Binet [a], Bruno Viana [a], Didier Gourier [a,*]

[a] Institut de Recherche de Chimie-Paris, CNRS – Chimie-ParisTech, 11 rue Pierre et Marie Curie, 75005 Paris, France
[b] Department of Physics, Goa University, Goa 403206, India

ARTICLE INFO

Article history:
Received 18 March 2014
Received in revised form
26 June 2014
Accepted 27 June 2014
Available online 5 July 2014

Keywords:
Optical materials
Long lasting phosphorescence
in vivo optical imaging
Solid state synthesis
Thermally stimulated luminescence

ABSTRACT

In the quest of bright and long persistent far-red/near-infrared phosphors for in vivo optical imaging, the interest in the family of $ZnGa_2O_4$ spinel compounds doped with Cr^{3+} has been aroused in the most recent years. We show that the dopant concentration plays an important role in the total persistent luminescence output of the material. $ZnGa_2O_4$ doped with 0.25%, 0.50% and 0.75% Cr relative to (Ga+Cr) was prepared by solid state synthesis. 0.50% Cr was found optimal to obtain the most intense persistent luminescence after matrix excitation with X-rays or localized excitation in Cr^{3+} absorption band with 550 nm wavelength. Up to 0.5% Cr content, persistent luminescence increases as a consequence of an increased number of Cr^{3+} luminescent centers and associated defects. With 0.75% Cr content, a too large number of defects locally concentrated around Cr^{3+} ions are detrimental to the long-term persistent luminescence intensity. We supplement long lasting phosphorescence investigation with laser excited photoluminescence and thermally stimulated luminescence results.

1. Introduction

$ZnGa_2O_4$ (ZGO) is a large band gap (4.5 eV) semiconductor with normal spinel structure [1,2]. In the 1990s it was reported for applications in vacuum fluorescent displays and field emission displays as the material was shown to present a broad blue emission band at 470 nm with excellent cathodoluminescence characteristics at low voltage and a perfect thermal stability [3,4]. It also drew attention as a novel UV transparent electronic conductor and as one of the most interesting substrates for GaN deposition to make thin films electroluminescent devices [5,6]. Doped with transition metal ions such as Mn^{2+} or Cr^{3+} the material turns into a phosphor emitting a bright green or red luminescence, respectively [7–9]. As a red phosphor emitting in the range 660–720 nm, Cr^{3+}-doped $ZnGa_2O_4$ (ZGO:Cr) aroused interest in bio-imaging application. Furthermore ZGO:Cr was recently discovered to exhibit an intense persistent luminescence – also called long-lasting phosphorescence (LLP) – i.e. to continue emitting light for hours after the end of an excitation [10]. Therefore we showed that ZGO:Cr nanoparticles presented ideal properties to play the role of persistent luminescence bio-markers and realize in vivo imaging of small animals using a cost-effective and harmless technique [11]. Indeed mammal tissues present a maximum transparency to light in the 650–1100 nm wavelength range [12]. Compared to first generation LLP bio-markers such as $Ca_{0.2}Zn_{0.9}Mg_{0.9}Si_2O_6:Eu^{2+}$, Mn^{2+}, Dy^{3+} [13] and $CaMgSi_2O_6:Eu^{2+}$, Mn^{2+}, Pr^{3+} [14] used for the proof of concept, ZGO:Cr family presents outstanding persistent luminescence properties after UV and visible light excitation [10,15–17]. The latter was shown to enhance the imaging capabilities of LLP phosphors since ZGO:Cr nanoparticles could be excited in vivo several times by orange excitation and enable long-term imaging necessary to the detection of carcinogenic tumors [16].

Considering the remarkable properties of this far-red/near infrared (NIR) persistent phosphor, the interest in ZGO:Cr has been aroused further in the most recent months. On the one hand, ZGO:Cr has become a compound of choice to investigate persistent luminescence mechanism [17,18] and on the other hand some interesting attempts to further enhance efficiency have been proposed. The following procedures have been reported as successful ways to improve LLP light yield/decay time duration: (i) a 1% ZnO deficiency in the reactants medium [10,18], (ii) a gallium substitution by tin or germanium [15,19], (iii) a co-doping by bismuth [20], and (iv) Cr^{3+}/Pr^{3+} codoping in gallogermanates [21]. It is interesting to note that all these materials were doped with chromium ions. However, we believe that the Cr content should also be checked for optimization of persistent luminescence which is not reported so far to best of our knowledge.

* Corresponding author. Tel.: +33 153737941.
E-mail address: didier.gourier@chimie-paristech.fr (D. Gourier).

http://dx.doi.org/10.1016/j.jlumin.2014.06.056
0022-2313/

The object of the present work is to investigate the influence of the chromium content in ZGO:Cr. The study will establish the interplay between the chromium concentration for most intense persistent luminescence and the presence of quenching structural defects.

2. Materials and methods

Four ZGO:Cr samples were prepared by a solid state method. A nominal 1% Zn deficiency relative to stoichiometry was introduced in the reactants ratio (Zn/(Ga+Cr)=0.495) as this was shown to yield enhanced LLP and to manage the structural disorder [10,18]. One un-doped and three doped samples with 0.25, 0.50 and 0.75 at% Cr relative to (Ga+Cr) were prepared. Appropriate amounts of zinc oxide (ZnO), gallium oxide (Ga_2O_3) and chromium trioxide (CrO_3) were mixed and ground in an agate mortar with isopropan-2-ol to obtain 1 g final product. The mixtures were dried at 60 °C to evaporate excess alcohol. 1 cm-diameter pellets were pressed before annealing in air at 1300 °C for 6 h. The samples were carefully ground before any measurement. It is important to note that the oxidation state of Cr in the starting doping CrO_3 is 6+. However, CrO_3 decomposes above 197 °C liberating oxygen and gives Cr_2O_3 following the reaction: $4\ CrO_3 \rightarrow 2\ Cr_2O_3 + 3\ O_2$ [22]. As our samples were annealed at much higher temperature, an obvious decomposition is expected. The lack of Cr in 4+, 5+ and 6+ valence states was checked by reflectance, photoluminescence and EPR, as discussed in later sections.

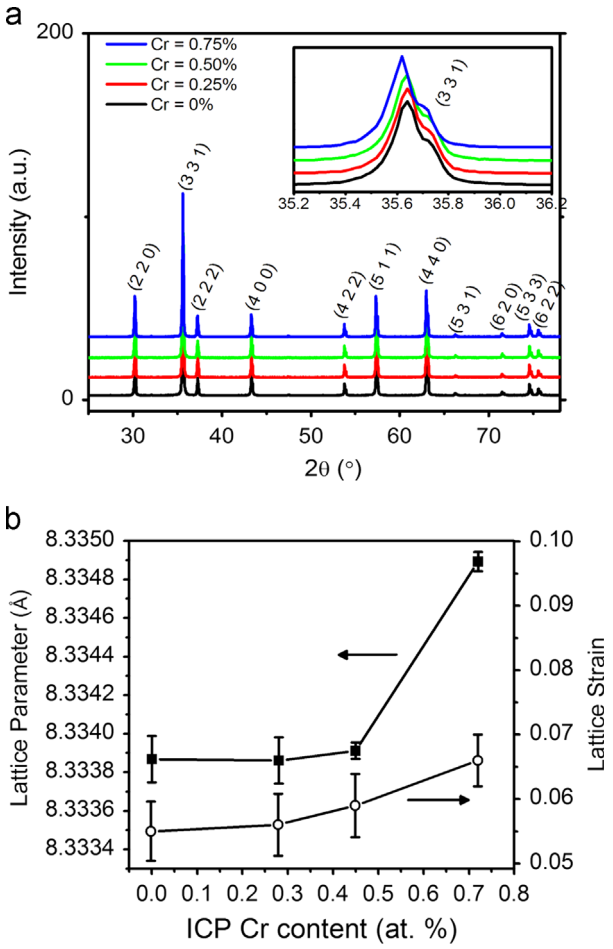

Fig. 1. (a) X-ray diffraction pattern of undoped and chromium-doped $ZnGa_2O_4$. The inset shows an expanded view of the (331) diffraction peak. (b) Variation of lattice parameter and lattice strain with chromium concentration measured by ICP-AES.

X-ray diffraction (XRD) patterns were recorded with a Rigaku X-ray diffractometer working with CuKα radiation (λ=1.5406 Å) and equipped with a horizontal goniometer. The diffractograms were recorded at a scan speed of 2°/min and a step size of 0.02° over a wide 2θ range (20–80°). Inductively coupled plasma-atomic emission spectroscopy (ICP-AES) was performed on iCAP 6000 series emission spectrometer with charge injection device (CID) detector RACID86. Prior to ICP-AES measurement, overnight refluxing at 120 °C was performed to dissolve 10 mg powder sample into 10 ml 51% HNO_3 aqueous solution. Standard Cr solution from SCP Science (number S110505001) was used to prepare solutions for calibration curve. Diffuse reflectance was measured by a Varian Cary UV–vis–NIR spectrophotometer 6000i. The light from a halogen lamp for visible range (> 360 nm) and deuterium lamp for UV range (< 360 nm) is passed through a monochromator before it reaches an integrating sphere containing the sample and a barium sulfate standard (for baseline correction). The powders were firmly packed into a 1.5 cm diameter sample holder and mounted on the sample port of the integrating sphere. Pulsed laser excited photoluminescence (PL) was run on 6 mm-diameter pellets (50 mg powder) silver glued on the cold finger of a cryogenic system and maintained at 20 K. The emitted light was collected by an optical fiber and transmitted to a Scientific Pixis 100i CCD camera cooled at −20 °C and coupled to a monochromator with 1200 groves/mm grating. The pellets were excited by an optical parametric oscillator (OPO) pumped by the tripled excitation of a YAG:Nd laser. The PL spectra were measured with 10 ms gate width and 26 ns gate delay. X-band (~9.45 GHz frequency) and Q-band (~35 GHz) electron paramagnetic resonance (EPR) measurements were performed at room temperature on weight normalized samples using a Bruker Elexsys E500 continuous wave EPR spectrometer. Simulations of EPR spectra were performed using X-Sophe software tool from Bruker. LLP was measured at room temperature (295 K) on 180 mg powder samples packed into a 1 cm-diameter sample holder. Emitted light was collected via an optical fiber with a Scientific Pixis 100 CCD camera cooled at −65 °C coupled with an Acton SpectraPro 2150i spectrometer for spectral analysis. Two types of excitation, X-rays (Mo-tube, 20 mA – 50 kV, λ=0.66729 ± 0.0463 Å) and green laser light from the OPO (λ=550 nm, 10 mJ, pulse width 4 ± 1 ns) were used to excite LLP. Excitation and luminescence were performed at 45° angle from the sample surface thereby making a total 90° angle between excitation and detection. All the samples were bleached at 250 °C for 20 min and kept in the dark prior to any LLP measurement.

3. Results and discussion

The XRD patterns of the four samples are shown in Fig. 1(a). They all present the expected diffraction peaks of ZGO spinel with the Fd3m cubic space group. The un-doped and all doped samples exhibit no impurity phases. The position and width of the peaks are identical for the 0%, 0.25% and 0.50% Cr-doped samples, evidencing no structural change or disorder with the introduction of up to 0.50% Cr in ZGO structure. The XRD peaks of the 0.75% Cr-doped sample are slightly shifted towards small angles (see the inset of Fig. 1(a)). The lattice parameters calculated using Rietveld refinement and the lattice strain evaluated using the Williamson–Hall method are reported in Fig. 1(b). The abscissa of Fig. 1 (b) displays the samples chromium content measured by ICP-AES. The latter for the nominal 0.25% Cr-doped sample was found to be 0.28 ± 0.01%, i.e. slightly higher than the nominal value. For the two other Cr-doped samples, the value measured by ICP-AES is

slightly lower than the nominal values ($0.45 \pm 0.01\%$ vs. 0.50% and $0.72 \pm 0.01\%$ vs. 0.75%). The difference between ICP-AES and nominal values is ascribed to experimental uncertainties in ICP-AES measurement and/or in sample preparation. However, the differences remain small which enabled us to consider that all chromium was globally introduced into the samples. In Fig. 1(b), the lattice parameter is identical (8.33388 Å) for the 0%, 0.25% and 0.50% Cr-doped samples. A slight increase of lattice parameter (+ 0.01%) is observed for 0.75% Cr-doped sample. Similarly the lattice strain is close to 0.056 for the un-doped, 0.25% and 0.50% Cr-doped samples whereas it increases to 0.067 for the 0.75% Cr-doped sample. Finally, the XRD analysis shows that no crystal disorder can be observed when chromium is introduced up to 0.50%, and a weak disorder is evidenced for the 0.75% Cr-doped sample by a slight increase of lattice parameter and lattice strain. It is to be remembered here that the ionic radii of hexa-coordinated [Cr^{3+}] and [Ga^{3+}] are identical (0.63 Å).

Fig. 2 shows experimental X-band (~9.4 GHz) EPR spectra of the four samples together with a simulated spectrum for the 0.50% Cr-doped compound. All the spectra could be simulated by considering only Cr^{3+} ($3d^3$), which means that there is no trace of Cr^{5+} ($3d^1$) with $S=1/2$. EPR simulation of unperturbed Cr^{3+} ion ($S=3/2$) in ZGO host was performed with the following spin Hamiltonian in trigonal symmetry:

$$H = g_{//}\beta B_z S_z + g_{\perp}\beta(B_x S_x + B_y S_y) + D\left[S_z^2 - S(S+1)/3\right]$$

where the first two terms represent the electron Zeeman interaction and the third term the axial zero field splitting (ZFS) interaction. The simulation of the spectrum of the 0.50% Cr-doped sample could be performed with the same ZFS parameter $D=0.524\ cm^{-1}$ and g-factors $g_{//}=1.9774$ and $g_{\perp}=1.9761$ =as reported for $ZnGa_2O_4$: Cr single crystals [23]. In the experimental spectra of the three Cr-doped samples, an additional signal was observed at 198.4 mT (indicated by arrows in Fig. 2). Its intensity was found to increase with Cr concentration and was thus ascribed to Cr^{3+}–Cr^{3+} pairs. The main absorption line of Cr^{3+} at 174.1 mT is enlarged in the inset of Fig. 2 for the three experimental spectra of Cr-doped weight normalized samples. When Cr concentration increases from 0.25% to 0.5%, the intensity increase of the line is observed evidencing a doubled content of Cr^{3+} in substitution of Ga^{3+}, with a similar environment around Cr^{3+} ions. From 0.50% to 0.75% the evolution is different since the EPR line broadens without increasing its intensity and the absorption maximum slightly shifts to higher magnetic field (~0.8 mT). Those features are ascribed to crystal field distortions around Cr^{3+} ions, in agreement with XRD.

Fig. 3 shows variation of the 174.1 mT line intensity as a function of Cr content determined by ICP-AES. The line intensity was calculated as the peak-to-peak amplitude multiplied by the square of the peak-to-peak width of the line. It is found to linearly increase with the Cr content. While ICP-AES measures chromium content under any oxidation state, EPR measures only Cr^{3+}. The linear variation of the EPR intensity with chromium content means that all Cr atoms are introduced as Cr^{3+} ions substituting Ga^{3+} into the ZGO structure. This is most probably due to the excellent matching between Cr^{3+} and Ga^{3+} cationic radii.

The resolution of EPR can be improved at higher frequency. Fig. 4 presents the Q-band (~35 GHz) EPR spectrum for 0.75% doped sample (black line). The spectrum showed several intense EPR lines which are well reproduced in the spectrum simulated with the same axial spin Hamiltonian parameters as for X-band spectrum (red line in Fig. 4). As for X-band, the Q-band spectrum is dominated by Cr^{3+} in unperturbed Ga^{3+} sites of ZGO. The small D value ($0.524\ cm^{-1}$) is due to the weak trigonal symmetry of this site. The spectrum is dominated by 5 lines, with three lines corresponding to magnetic field orientation $\boldsymbol{B}_0 \perp C_3$ (~108 mT,

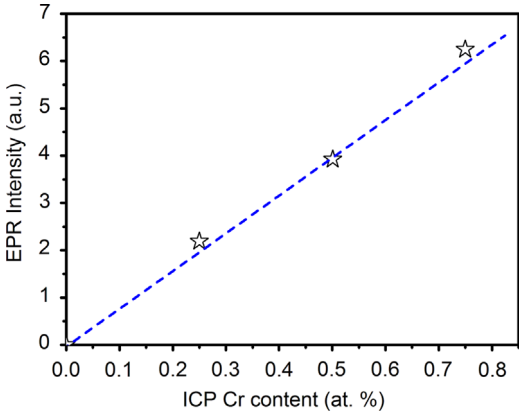

Fig. 3. Intensity of the X-band EPR line of Cr^{3+} at 174 mT vs. chromium content measured by ICP in $ZnGa_2O_4$.

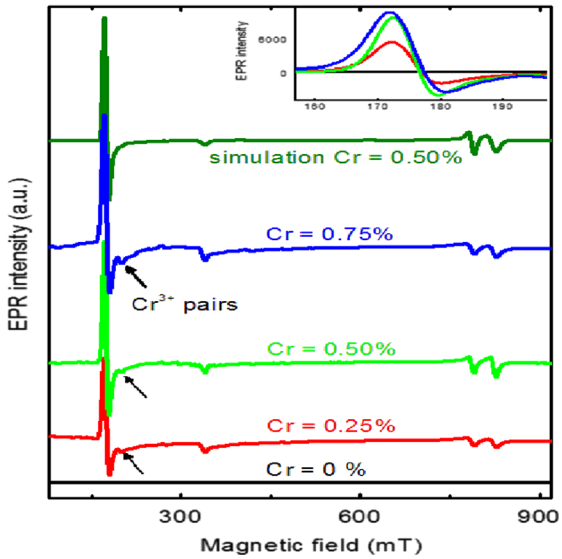

Fig. 2. X-band EPR spectra at room temperature of 0%, 0.25%, 0.50% and 0.75% Cr-doped $ZnGa_2O_4$, compared with a spectrum simulated for Cr^{3+} in undistorted Ga^{3+} site of the structure. The low field line is expanded in the inset.

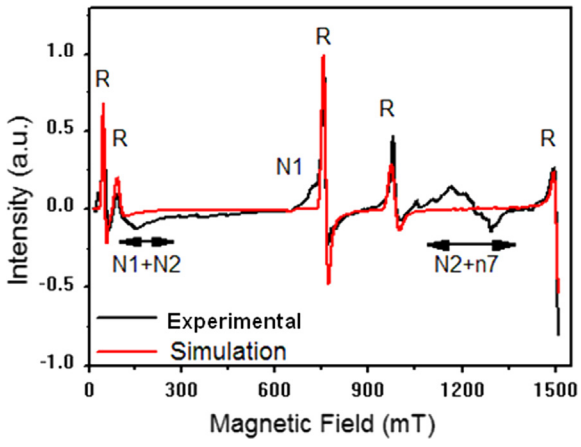

Fig. 4. Experimental Q-band EPR spectrum at room temperature of 0.75% Cr doped $ZnGa_2O_4$ (black line) compared with spectrum simulated for Cr^{3+} in undistorted Ga^{3+} sites of the compound (red line). EPR lines of this undistorted site are noted R. Additional lines in the experimental spectrum correspond to Cr^{3+} with neighboring defects, noted N1, N2, and n7 according to the notation of the corresponding optical emission lines (For interpretation of the references to color in this figure legend, the reader is referred to the web version of this article).

~765 mT, ~984 mT), one line corresponding to $\boldsymbol{B}_0$ oriented at 30–40° from C_3 axis (~1495 mT) and one line at low magnetic field (~55 mT) corresponding to a broad range of magnetic field orientations [18]. Other weaker lines appear in the flanks of main lines or between them, showing the presence of other type of Cr^{3+} ions. These additional spectra can be simulated by considering non-axial component of the ZFS, indicating that these other Cr^{3+} ions are weakly perturbed by neighboring defects [18]. These lines are labeled in Fig. 4 as N1, N2 and n7 according to correlation previously proposed with optical emission lines [18]. We infer that as the Cr concentration is increased, the populations of structural defects increase due to an increased lattice strain also reflected by the increase in lattice parameters.

UV–visible diffuse reflectance spectra are shown in Fig. 5. In the spectrum of the undoped sample, the O^{2-}–Ga^{3+} charge transfer band (band gap absorption) of ZGO host is observed peaking at 245 nm. From Tauc's law [24], the band gap is evaluated to 4.5 eV and is in agreement with literature [1]. The spectra of Cr doped samples present two additional absorption bands at 550 nm and 420 nm attributed to $^4A_2$ (^4F)→$^4T_2$ (^4F) and $^4A_2$ (^4F)→$^4T_1$ (^4F) transitions of Cr^{3+}, respectively. A third band, partly superimposing with ZGO band gap edge, can be distinguished around 300 nm. We attribute this band to the third spin-allowed $^4A_2$ (^4F)→$^4T_1$ (^4P) absorption transition of Cr^{3+}, whose maximum is expected at around 260 nm according to a Tanabe Sugano diagram for a d^3 ion [25]. The three observed d–d bands consistently show an increasing intensity with Cr^{3+} content. We can note the absence of Cr^{6+} impurities deduced from the lack of O^{2-}–Cr^{6+} charge transfer, which should give an intense transition around 360 nm [26]. Also there are no additional absorption bands in the visible that could be attributed to d–d transitions of Cr^{4+} or Cr^{5+}.

The room temperature PL excitation and emission spectra of ZGO:Cr compounds are shown in Fig. 6. The excitation spectra show similar features to the reflectance spectra of Fig. 5, i.e. an O^{2-}→Ga^{3+} charge-transfer band at 245 nm and three d–d bands of Cr^{3+} at 550 nm ($^4A_2$ (^4F)→$^4T_2$ (^4F)), 420 nm ($^4A_2$ (^4F)→$^4T_1$ (^4F)), and 300 nm ($^4A_2$ (^4F)→$^4T_1$ (^4P)). The bands at 420 nm and 550 nm show double humps or broadening. This is mainly due to the trigonal distortion and spin–orbit coupling at Ga^{3+} site which split the Cr^{3+} excited states [10]. The emission spectra, magnified in the inset, are composed of emission lines due to the ^2E (^4F)→$^4A_2$ (^4F) transition of Cr^{3+}. An emission spectrum is made of zero phonon lines (ZPL) accompanied by their phonon side bands (PSB). In the inset of Fig. 6 the ZPL of Cr^{3+} in undistorted Ga^{3+} sites is identified at 687 nm (R-lines) with accompanying Stokes PSB (S-PSB) at 707 nm and 713 nm and anti-Stokes PSB (AS-PSB) at 669 nm and 679 nm. The ZPL of Cr^{3+} ions distorted by an antisite defects as first cationic neighbor is identified at 693 nm (N2 line) [17,27–30]. The three spectra were normalized at N2 emission line.

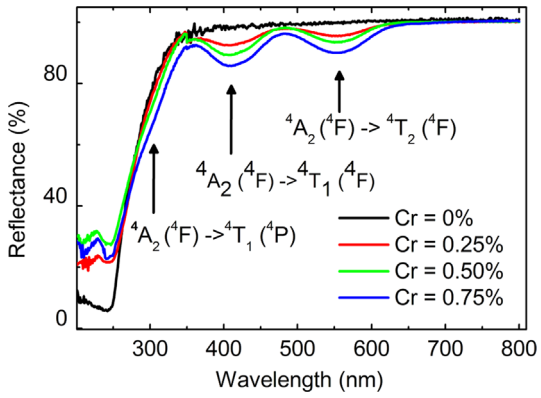

Fig. 5. Diffuse reflectance spectra of undoped and Cr-doped $ZnGa_2O_4$.

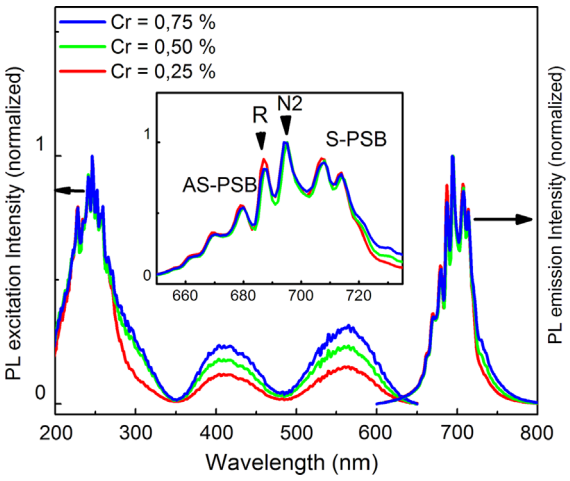

Fig. 6. Room temperature photoluminescence spectra (right) and their excitation spectra (left) for chromium-doped $ZnGa_2O_4$. The emission spectrum is enlarged in the inset, and shows the zero-phonon lines of undistorted (R) and distorted (N2) Cr^{3+} sites, flanked by anti-Stoke (AS) and Stoke (S) phonon side bands (PSB).

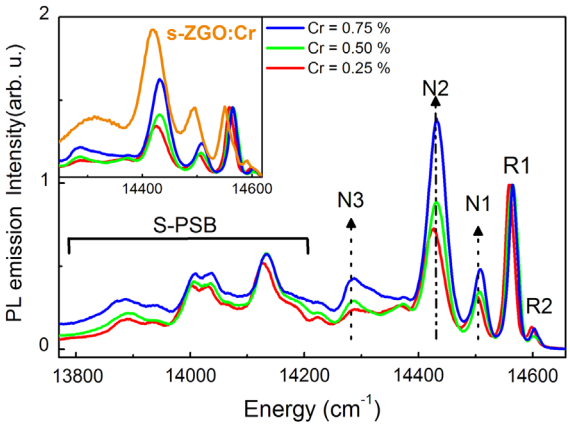

Fig. 7. Laser excited photoluminescence spectra at 20 K of chromium doped $ZnGa_2O_4$ synthesized with Zn/(Ga+Zn)=0.55. The zero-phonon lines labeled R1/R2, N1, N2 and N3 correspond to the different types of Cr^{3+}. The inset shows a zoom of the emission range N1–R2 compared with the emission spectrum of a 0.50% Cr-doped sample synthesized with nominal composition Zn/(Ga+Zn)=0.50 (labelled s-ZGO:Cr).

The N2/R ratio appears slightly smaller for the 0.25% Cr-doped sample than for the highest Cr content samples.

As emission lines are broadened at room temperature, the effect of Cr^{3+} concentration on N2/R ratio was examined into more detail by laser excited PL experiments carried out at 20 K. Spectra are shown in Fig. 7. The spectra now present distinct R1 and R2 lines at 14,555 and 14,595 cm^{-1} (ideal Cr^{3+}), ascribed to the splitting of Cr^{3+} ^2E excited state into two levels separated by ~40 cm^{-1} and due to trigonal distortion. N1, N2 and N3 lines were identified at 14,501 cm^{-1}, 14,421 cm^{-1} and 14,275 cm^{-1}, respectively [29,30]. The latter has been unambiguously attributed to Cr^{3+}–Cr^{3+} pairs, i.e. Cr^{3+} ions at neighboring cationic sites [28,31], whereas several attributions have been proposed for N1 line. The most credible attributions propose an antisite defect at Zn site on C_3-axis as first cationic neighbor to Cr^{3+} (Ga°_{Zn}) [18,30] or Zn vacancy [27] or to a Cr^{3+}–Zn_i pair (Zn_i is an interstitial Zn) [32]. Lines at 14,128 cm^{-1} and 14,025 cm^{-1}, 13,994 cm^{-1} are attributed to S-PSB of R-lines. As expected from low temperature measurements, no AS-PSB emission is observed at 20 K. All the graphs are normalized with respect to R1 line. The series of Cr^{3+} doped samples then shows a monotonous N2/R ratio trend (0.73, 0.90 and 1.39 for 0.25%, 0.50% and 0.75% Cr doped samples,

respectively). Therefore the number of Cr^{3+}–Cr^{3+} pairs (N3) but also of antisite defects (N1 and N2) increase around Cr^{3+} when the chromium content of the samples increases. However, it is important to note that this increase remains moderate compared to other ways to introduce defects into ZGO structure without modifying the chromium content. Indeed one of our previous studies showed that slightly modifying the nominal Zn/Ga cationic ratio had a much larger effect on the number of defects around Cr^{3+} ions. This is shown in the inset of Fig. 7 where a nominally stoichiometric compound (named s-ZGO:Cr) prepared with Zn/(Ga+Cr)=0.5 (instead of here Zn/(Ga+Cr)=0.5495) and a 0.50% Cr content presents a much higher N2/R ratio (~2.1) [17]. Therefore the distortion introduced in the lattice with increasing Cr content up to 0.75% can be considered as moderate.

Fig. 8 shows the X-ray excited optical luminescence (XREOL), the X-ray excited long-lasting phosphorescence (XELLP) and the green light excited long-lasting phosphorescence (GELLP) spectra normalized at R-line intensity for the Cr-doped samples. The XREOL spectra show R line and N2 line at 14,550 cm^{-1} and 14,420 cm^{-1}, respectively. The R-line could not be resolved to its respective R1 and R2 components due to poor instrument resolution and room temperature measurement. S-PSB of R-line is observed at 14,127 cm^{-1} and 14,026 cm^{-1} and AS-PSBs of R-line at 14,719 cm^{-1} and 14,930 cm^{-1}. The N2/R ratio slightly increases with the increase in Cr concentration in agreement with the laser excited PL results at low temperature (Fig. 7). Nevertheless the differences in N2/R ratio are much more moderate in Fig. 8 since (a) the line resolution is lower due to the set-up and to room temperature measurement, and (b) PSB are more intense and AS-PSB are present. As already observed, LLP emission spectra are largely dominated by the N2 line with very little contribution from the R line and its PSB for all the samples [10,17,18].

The LLP decay curves for the three Cr-doped samples are shown in Fig. 9. X-rays (noted X-exc) were chosen for host lattice excitation and 550 nm green light was chosen for direct Cr^{3+} excitation ($^4A_2$ (^4F) → $^4T_2$ (^4F) transition). Indeed it was shown that ZGO:Cr is a persistent luminescence phosphor that can be excited by virtually all visible wavelength by exciting the d–d absorption bands of Cr^{3+} [16,17]. The results in Fig. 9 show that 0.50% Cr content is an optimum concentration to obtain intense persistent luminescence irrespective of the excitation energy used. The thermally stimulated luminescence (TSL) glow curves were obtained at 230 nm laser excitation and 5 min excitation time.

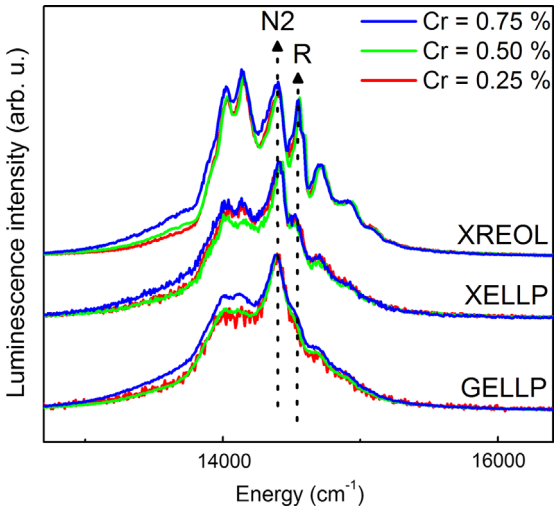

Fig. 8. Comparison of X-ray excited optical luminescence (XREOL), X-ray excited long lasting phosphorescence (XELLP) and green-light excited long lasting phosphorescence (GELLP) in $ZnGa_2O_4$ with three chromium concentrations.

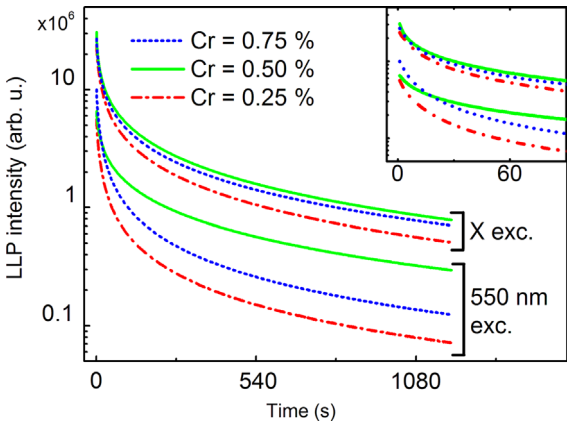

Fig. 9. LLP decay after X-ray excitation (X exc.) and after green light excitation (550 nm exc.) in $ZnGa_2O_4$ for three chromium concentrations. The inset shows the decays at short times.

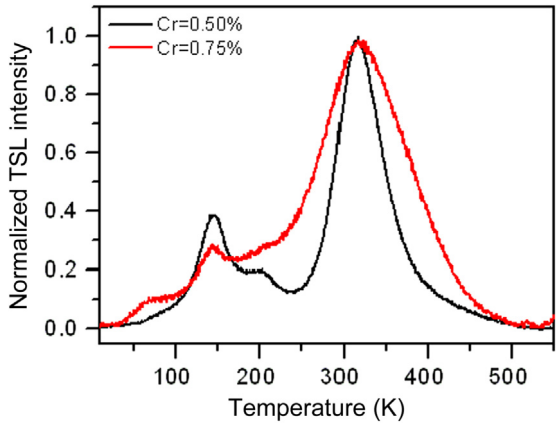

Fig. 10. Thermally stimulated luminescence (TSL) curve of 0.50 at% and 0.75% chromium-doped $ZnGa_2O_4$, excited at 230 nm (5 min duration).

The normalized TSL glow curves for 0.50% and 0.75% are compared in Fig. 10. The main TSL peak observed around 317 K is responsible for the long LLP in ZGO:Cr^{3+}. This TSL peak broadens with the increase in Cr concentration (FWHM of 67 K and 125 K for 0.50% and 0.75% Cr concentration, respectively). We infer that the quasi-continuous distribution of traps with activation energy between 0.6 and 0.9 eV [17] and their overall population increases with Cr concentration. The samples also possess shallower traps (with activation energy ~0.5 eV). All the samples have the same glow curve structure suggesting increase in population of the same types of defects and no new defects are formed in the crystal lattice as the Cr concentration is increased and/or as a side effect of excitation with X-rays.

Going into more detail, the LLP of ZGO:Cr is largely enhanced by moving from 0.25% to 0.50% Cr. We observed no global disorder by XRD and no local disorder around Cr^{3+} ions by optical and EPR spectroscopy upon increasing Cr content from 0.25% to 0.50%. However the chromium concentration indeed doubles. Therefore, the large LLP enhancement observed is mostly due to the doubling number of emitting Cr^{3+} ions with their associated defects since persistent luminescence in ZGO:Cr was shown to originate from defects located in the neighborhood of Cr^{3+} ions [10,16–18].

When nominal Cr content increases from 0.50% to 0.75% Cr, LLP intensity globally decreases except at the very beginning of the decay (cf. Fig. 9 and inset). Yet we showed that the real Cr content increased linearly with the nominal introduction of chromium. However, structural changes also occurred. XRD patterns showed

that a global structural disorder was introduced. EPR and optical spectroscopy showed that many Cr–Cr pairs were formed and that the number of Cr^{3+} ions possessing antisite defects in their immediate environment was increasing, as assessed by the increased intensity of N1 and N2 lines in low temperature photoluminescence spectra. We previously showed that such an increased disorder, controlled by the Zn/Ga nominal ratio at constant 0.5% Cr concentration, was the cause of an increased LLP intensity in the first two minutes of decay together with decreased persistent luminescence intensity afterwards [18]. Therefore here, in spite of a probably favorable increase in the number of Cr^{3+} ions, a 0.75% Cr content in ZGO:Cr is globally unfavorable to LLP due to the co-introduction of structural disorder. This disorder concentrates locally around Cr^{3+} ions and consequently affects even more persistent luminescence excited with 550 nm light than LLP excited with X-rays. An observed accelerated decay of persistent luminescence in the first minute for 0.75% Cr content (see the inset in Fig. 9) is typical from non-radiative recombination of charges located at concentrated defects, i.e. at defects very close to each other [30].

4. Conclusion

We investigated the influence of chromium concentration on the phenomenon of persistent luminescence in ZGO:Cr. Similarly to what has already been observed in 0.5% Cr doped ZGO, persistent luminescence of more (0.75%) or less (0.25%) highly doped compounds also present a spectrum largely dominated by Cr_{N2} ions. This has been explained by a LLP mechanism whereby carriers are generated at clusters formed by Cr^{3+} ions and neighboring pairs of antisite defects [17,18]. This localization of defects around Cr^{3+} ions enables the formation, trapping and emission, and consequently allows us to observe persistent luminescence in ZGO:Cr excited with 550 nm green light. In the present study we showed by EPR and ICP-AES measurements that chromium was quantitatively introduced in zinc gallate structure up to the highest Cr content (0.75%) under the unique form of Cr^{3+} ions substituting Ga^{3+}. XRD, EPR and low temperature optical spectroscopy showed that structural disorder was increased for 0.75% Cr content with overall an increased number of Cr^{3+} ions with antisite neighboring defects. As a consequence, the 0.50 at% concentration (relative to Ga+Cr) was found to be the optimal chromium concentration in ZGO:Cr to obtain the most intense persistent luminescence after host lattice excitation (X-rays) or excitation in Cr^{3+} absorption bands (visible light).

Acknowledgment

The authors are grateful to the Indo-French Centre for the Promotion of Advanced Research (IFCFAR)/Centre Franco-Indien Pour la Recherche Avancée (CEFIPRA) for the financial support (Project 4508-1). The authors acknowledge Patrick Aschehoug and Laurent Michely for experimental help.

References

[1] S.Zh. Karazhanov, P. Ravindran, J. Am. Ceram. Soc. 93 (2010) 3335.
[2] D. Errandonea, R. Kumar, F. Manjón, V. Ursaki, E. Rusu, Phys. Rev. B 79 (2009) 024103.
[3] I.J. Hsieh, K.T. Chu, C.F. Yu, M.S. Feng, J. Appl. Phys. 76 (6) (1994) 3735.
[4] S. Itoh, H. Toki, Y. Sato, K. Morimoto, T. Kishino, J. Electrochem. Soc. 138 (1991) 1509.
[5] T. Omata, N. Ueda, K. Ueda, H. Kawazoe, Appl. Phys. Lett. 64 (9) (1994) 1077.
[6] A.R. Phani, S. Santucci, S.D. Nardo, L. Lozzi, M. Passacantando, P. Picozzi, C. Cantalini, J. Mater. Sci. 33 (1998) 3969.
[7] L.E. Shea, R.K. Datta, J.J. Brown Jr., J. Electrochem. Soc. 141 (1994) 1950.
[8] H.M. Kahan, R.M. Macfarlane, J. Chem. Phys. 54 (12) (1971) 5197.
[9] T. Ohtake, N. Sonoyama, T. Sakata, Chem. Phys. Lett. 318 (2000) 517.
[10] A. Bessière, S. Jacquart, K. Priolkar, A. Lecointre, B. Viana, D. Gourier, Opt. Express 19 (2011) 10131.
[11] T. Maldiney, C. Richard, D. Scherman, D. Gourier, B. Viana, A. Bessière, Patent FR2012-1250846, 30/01/2012.
[12] R. Weissleder, V. Ntziachristos, Nat. Med. 9 (2003) 123.
[13] Q. Le Masne de Chermont, C. Chanéac, J. Seguin, F. Pelle, S. Maitrejean, J.-P. Jolivet, D. Gourier, M. Bessodes, D. Scherman, Proc. Natl. Acad. Sci. U.S.A. 104 (2007) 9266.
[14] T. Maldiney, A. Lecointre, B. Viana, A. Bessière, M. Bessodes, D. Gourier, C. Richard, D. Scherman, J. Am. Chem. Soc. 133 (2011) 11810.
[15] Z. Pan, Y.Y. Lu, F. Liu, Nat. Mater. 11 (2012) 58.
[16] T. Maldiney, A. Bessière, J. Seguin, E. Teston, S.K. Sharma, B. Viana, A.J.J. Bos, P. Dorenbos, M. Bessodes, D. Gourier, D. Scherman, C. Richard, Nat. Mater. 13 (2014) 418.
[17] A. Bessière, S.K. Sharma, N. Basavaraju, K.R. Priolkar, L. Binet, B. Viana, A.J.J. Bos, T. Maldiney, C. Richard, D. Scherman, D. Gourier, Chem. Mater. 26 (2014) 1365.
[18] D. Gourier, A. Bessière, S.K. Sharma, L. Binet, B. Viana, N. Basavaraju, K. R. Priolkar, J. Phys. Chem. Solids 75 (2014) 826.
[19] M. Allix, S. Chenu, E. Véron, T. Poumeyrol, E.A.K. Boudjelthia, S. Alahraché, F. Porcher, D. Massiot, F. Fayon, Chem. Mater. 25 (2013) 1600.
[20] Y. Zhuang Ueda, S. Tanabe, Appl. Phys. Express 6 (2013) 052602.
[21] A. Abdukayam, J.T. Chen, Q. Zhao, X.P. Yan, J. Am. Chem. Soc. 135 (2013) 14125.
[22] R.S. Schwartz, I. Fankuchen, R. Ward, J. Am. Chem. Soc. 74 (7) (1952) 1676.
[23] H.V. Boom, J.C.M. Henning, J.P.M. Damen, Solid State Commun. 8 (1970) 717.
[24] J. Tauc, Mater. Res. Bull. 3 (1968) 37.
[25] Y. Tanabe, S.J. Sugano, Phys. Soc. Jpn. 9 (1954) 766.
[26] C.z. Koepke, K. Winiewski, M. Grinberg, J. Alloys Compd. 341 (2002) 19.
[27] W. Nie, F.M. Michel-Calendini, C. Linares, G. Boulon, C. Daul, J. Lumin. 46 (1990) 177.
[28] J. Derkosch, W. Mikenda, J. Lumin. 28 (1981) 431.
[29] W. Mikenda, A. Preisinger, J. Lumin. 26 (1981) 53.
[30] W. Mikenda, A. Preisinger, J. Lumin. 26 (1981) 67.
[31] G.G.P. van Gorkom, J.M.C. Henning, R.P. van Stapele, Phys. Rev. B 8 (1972) 955.
[32] W. Zhang, J. Zhang, Z. Chen, T. Wang, S. Zheng, J. Lumin. 130 (2010) 1738.